SSD-TR-90-08

(4)

Ionospheric Conductivity Dependence of the Cross–Polar Cap Potential Difference and Global Joule Heating Rate

B.-H. AHN
University of Colorado
Boulder, CO. 80309-0449

Y. KAMIDE
Kyoto Sangyo University
Kyoto 603, Japan

S.-I. AKASOFU
University of Alaska
Fairbanks, AL. 99775-0800

H. W. KROEHL
National Geophysical Data Center
Boulder, CO. 80303

D. J. GORNEY
The Aerospace Corporation
El Segundo, CA. 90245-4691

31 October 1988

Prepared for

SPACE DIVISION
AIR FORCE SYSTEMS COMMAND
Los Angeles Air Force Base
P.O. Box 92960
Los Angeles, CA 90009-2960

LABORATORY OPERATIONS

The Aerospace Corporation functions as an "architect-engineer" for national security projects, specializing in advanced military space systems. Providing research support, the corporation's Laboratory Operations conducts experimental and theoretical investigations that focus on the application of scientific and technical advances to such systems. Vital to the success of these investigations is the technical staff's wide-ranging expertise and its ability to stay current with new developments. This expertise is enhanced by a research program aimed at dealing with the many problems associated with rapidly evolving space systems. Contributing their capabilities to the research effort are these individual laboratories:

Aerophysics Laboratory: Launch vehicle and reentry fluid mechanics, heat transfer and flight dynamics; chemical and electric propulsion, propellant chemistry, chemical dynamics, environmental chemistry, trace detection; spacecraft structural mechanics, contamination, thermal and structural control; high temperature thermomechanics, gas kinetics and radiation; cw and pulsed chemical and excimer laser development, including chemical kinetics, spectroscopy, optical resonators, beam control, atmospheric propagation, laser effects and countermeasures.

Chemistry and Physics Laboratory: Atmospheric chemical reactions, atmospheric optics, light scattering, state-specific chemical reactions and radiative signatures of missile plumes, sensor out-of-field-of-view rejection, applied laser spectroscopy, laser chemistry, laser optoelectronics, solar cell physics, battery electrochemistry, space vacuum and radiation effects on materials, lubrication and surface phenomena, thermionic emission, photosensitive materials and detectors, atomic frequency standards, and environmental chemistry.

Electronics Research Laboratory: Microelectronics, solid-state device physics, compound semiconductors, radiation hardening; electro-optics, quantum electronics, solid-state lasers, optical propagation and communications; microwave semiconductor devices, microwave/millimeter wave measurements, diagnostics and radiometry, microwave/millimeter wave thermionic devices; atomic time and frequency standards; antennas, rf systems, electromagnetic propagation phenomena, space communication systems.

Materials Sciences Laboratory: Development of new materials: metals, alloys, ceramics, polymers and their composites, and new forms of carbon; nondestructive evaluation, component failure analysis and reliability; fracture mechanics and stress corrosion; analysis and evaluation of materials at cryogenic and elevated temperatures as well as in space and enemy-induced environments.

Space Sciences Laboratory: Magnetospheric, auroral and cosmic ray physics, wave-particle interactions, magnetospheric plasma waves; atmospheric and ionospheric physics, density and composition of the upper atmosphere, remote sensing using atmospheric radiation; solar physics, infrared astronomy, infrared signature analysis; effects of solar activity, magnetic storms and nuclear explosions on the earth's atmosphere, ionosphere and magnetosphere; effects of electromagnetic and particulate radiations on space systems; space instrumentation.

REPORT DOCUMENTATION PAGE

1a. REPORT SECURITY CLASSIFICATION Unclassified	1b. RESTRICTIVE MARKINGS
2a. SECURITY CLASSIFICATION AUTHORITY	3. DISTRIBUTION / AVAILABILITY OF REPORT Approved for public release; distribution unlimited.
2b. DECLASSIFICATION / DOWNGRADING SCHEDULE	
4. PERFORMING ORGANIZATION REPORT NUMBER(S) TR-0088(3940-06)-9	5. MONITORING ORGANIZATION REPORT NUMBER(S) SSD-TR-90-08
6a. NAME OF PERFORMING ORGANIZATION The Aerospace Corporation 6b. OFFICE SYMBOL (If applicable)	7a. NAME OF MONITORING ORGANIZATION Space Division Air Force Systems Command
6c. ADDRESS (City, State, and ZIP Code) 2350 E. El Segundo Blvd. El Segundo, CA 90245-4691	7b. ADDRESS (City, State, and ZIP Code) Los Angeles Air Force Base P. O. Box 92960 Los Angeles, CA 90009-2960
8a. NAME OF FUNDING / SPONSORING ORGANIZATION Space Division 8b. OFFICE SYMBOL (If applicable)	9. PROCUREMENT INSTRUMENT IDENTIFICATION NUMBER F04701-88-C-0089
8c. ADDRESS (City, State, and ZIP Code)	10 SOURCE OF FUNDING NUMBERS PROGRAM ELEMENT NO. / PROJECT NO. / TASK NO. / WORK UNIT ACCESSION NO.

11 TITLE (Include Security Classification)
Ionospheric Conductivity Dependence of the Cross-Polar Cap Potential Difference and Global Joule Heating Rate

12. PERSONAL AUTHOR(S)
B.-H. Ahn, Y. Kamide, S.-I. Akasofu, H. W. Kroehl, D. J. Gorney

13a. TYPE OF REPORT	13b. TIME COVERED	14. DATE OF REPORT (Year, Month, Day)	15. PAGE COUNT
Final	FROM _____ TO _____	31 October 1988	25

16. SUPPLEMENTARY NOTATION

17. COSATI CODES			18. SUBJECT TERMS (Continue on reverse if necessary and identify by block number)
FIELD	GROUP	SUB-GROUP	

19. ABSTRACT (Continue on reverse if necessary and identify by block number)

We examine the extent to which the cross-polar cap potential difference Φ and the global Joule heating rate U, both determined by the magnetogram - inversion method (Kamide et al., ~~1981~~), depend upon the assumed conductance models. For this purpose two statistically determined conductance models ~~developed by Spiro et al.~~ (1982) ~~and~~ Ahn et al. (1983~~b~~) and a realistic conductance distribution estimated from bremsstrahlung X-ray image data (~~Ahn et al. 1988~~) have been used. As expected from earlier studies, U is less affected by the choice of conductance models than is Φ. This is because U is a globally integrated quantity, and thus the local structures of the electric potential pattern do not affect it appreciably, whereas they are crucial in determining Φ, which is defined as the difference between the maximum and minimum potential values usually found in the dawn and dusk sectors, respectively. A comparison between U and Φ based on the statistical conductance models and U and Φ based on a
(continued)

20. DISTRIBUTION / AVAILABILITY OF ABSTRACT	21. ABSTRACT SECURITY CLASSIFICATION
☒ UNCLASSIFIED/UNLIMITED ☐ SAME AS RPT. ☐ DTIC USERS	
22a. NAME OF RESPONSIBLE INDIVIDUAL	22b. TELEPHONE (Include Area Code) / 22c OFFICE SYMBOL

realistic conductance distribution shows that there are considerable similarities, thus enabling us to use statistical conductance models as a first approximation in deriving such global quantities as the cross-polar cap potential difference and the global Joule heating in the study of solar wind-magnetosphere coupling. Several suggestions are made for improving the present available conductance models and some limitations (possibly intrinsic ones) are also discussed.

PREFACE

The numerical computation was done by computer at the National Center for Atmospheric Research, which is sponsored by the National Science Foundation. B.-H. A. acknowledges the generous hospitality of NOAA's National Geophysical Data Center and partial support from the Korea Science and Engineering Foundation.

CONTENTS

FIGURES

1. INTRODUCTION

It has been demonstrated that a network of ground-based magnetometers in the polar region can be considered as a "remote sensing tool" in estimating ionospheric quantities, such as ionospheric currents, field-aligned currents, the electric potential, and Joule heating rate (Akasofu and Kamide 1985). Furthermore, it is now possible to infer instantaneous patterns of such global distributions with a high-time resolution (say, 5 min.). In particular, the cross-polar cap potential difference Φ, estimated from the electric potential distribution, and the global Joule heating rate U are very useful in discussing the coupling between the solar wind and the earth's magnetosphere/ionosphere system, since they represent measures of the efficiency of penetration and dissipation of solar wind energy into the magnetosphere. For this purpose, several studies have correlated Φ and U thus obtained with geomagnetic indices (Ahn et al. 1984; Baumjohann and Kamide 1984; Kamide and Baumjohann 1986).

As already pointed out by Kamide and Richmond (1982), however, the electric potential distribution estimated primarily from the so-called magnetogram-inversion technique is very sensitive to the choice of ionospheric conductance models. Thus, it is highly desirable to examine the degree of dependence of these two quantities on the presently available conductance models. In the past there was no way to discuss quantitatively the uncertainties involved in Φ and U calculations, since no realistic conductance distribution was available. Fortunately, it has now become possible to infer a realistic conductance distribution using bremsstrahlung X-ray image data from satellites (Imhof et al, 1974, 1985, 1988; Mizera et al. 1978, 1984, 1985; Ahn et al. 1988), providing us with a unique opportunity to evaluate the errors by comparing the results (e.g., U and Φ) based on statistically determined conductance models, and the ones based on the realistic conductance distribution.

In this report, we calculate Φ and U by using the two statistically determined conductance models by Spiro et al. (1982) and Ahn et al. (1983) and the conductance distribution based on X-ray image data obtained from the DMSP

satellite. By comparing these results, we may gain some insight into how these quantities depend on different conductance distributions. Furthermore, it is of great interest to examine how closely such statistical models can simulate the realistic conductance distribution. This problem is particularly important because a direct estimation of ionospheric conductance, say from X-ray image data, is presently rarely available and most of the time we have to rely on one of the statistical models.

2. CONDUCTANCE MODELS

Recently several advanced conductance models (Wallis and Budzinski 1981; Spiro et al. 1982; Ahn et al 1983b; Craven et al. 1984; Kamide et al. 1986; Mishin et al. 1986; Fuller-Rowell and Evans 1987; Hardy et al. 1987) have been proposed, each based on an entirely different principle and using different data bases. In this study we choose to apply the Rice University model (Spiro et al. 1982) and the University of Alaska model (Ahn et al. 1983b).

The Rice University (RU) model is based on data of precipitating particle energy flux and average electron energy obtained from the AE-C and AE-D satellites, in which the conductance distribution is parameterized by the AE index. However, the conductance distribution may be significantly different at two instants with the same value of the AE index, particularly during individual substorms. To alleviate this effect, the following adjustment has been made before using the model in this study and in several previous studies (e.g., Kamide and Baumjohann 1985): The region of the most enhanced conductance zone is shifted latitudinally so that it coincides with the region of maximum equivalent current flow, whenever such a difference in latitude between the two maxima is found (for details, see Kamide et al. 1982a). The idea behind this latitudinal shift is that we assume that the location of the most intense auroral electrojet is the same as the location of the strongest auroral precipitation and thus of the highest ionospheric conductance. One may argue that the electrojet current may well be very strong where the conductance is relatively little enhanced but the electric field is very strong. From earlier studies, however, we know that this happens typically in the late morning sector, not in the midnight sector, where the substorm electrojet is most intense (Senior et al. 1982; Kamide et al. 1984). One may also argue that the equivalent currents may not accurately represent the "true" ionospheric currents. However, studies (e.g., Kamide et al. 1981) have shown that most of the equivalent currents represent reasonably well the true ionospheric currents at auroral latitude as far as their east-west component is concerned.

The University of Alaska (UA) model was devised by establishing empirical relationships between the Pedersen and Hall conductances deduced from Chatanika radar measurements and the magnitude of the simultaneous horizontal component of magnetic disturbances at College, Alaska. Although this model is considered statistical in the report, it is different from the RU model in that the conductance distribution is intended to reflect an instantaneous picture of the ionosphere by using instantaneous global magnetometer data as input; magnetic records from a total of 88 stations in the northern hemisphere are used in this study. Details of the method of constructing the instantaneous conductance distribution can be found in Ahn et al. (1983b).

Realistic instantaneous conductance distributions have been obtained from the DMSP-F6 satellite bremsstrahlung X-ray image data. The measured X-ray energy spectrum provides information about the precipitating electron spectrum (see, for example, Rosenburg et al. 1987), which is, in turn, used to compute the ionospheric conductance following the method of Vickrey et al. (1981). Although there are several shortcomings in estimating the large-scale ionospheric conductance distribution due to the orbital characteristics of the satellite and limitations of the instruments on board (for details, see Ahn et al. 1988), it is important to mention that the conductance distribution obtained through the X-ray data gives a two-dimensional instantaneous picture of the ionospheric conductance distribution. In our practical calculations, a background conductance of the solar UV origin has been added. For this we employed a revised version of the model presented by Kamide and Matsushita (1979).

For comparison, the Pedersen and Hall conductance distributions based on the three methods are shown in Figure 1 for the epoch of 2340-2355 UT on 23 July 1983. Since the Defense Meteorological Satellite Program (DMSP) satellite requires 17 min of scanning time for one hemisphere, the ground magnetic data were averaged over the period accordingly. The magnetic perturbation vectors at the epoch are shown in Figure 2 with the field view of the X-ray imager. The AE(12) index at the epoch, an input parameter of the RU model, recorded 712 nT. One can see clearly that the general features of the three distributions at auroral latitudes agree reasonably well. However, several

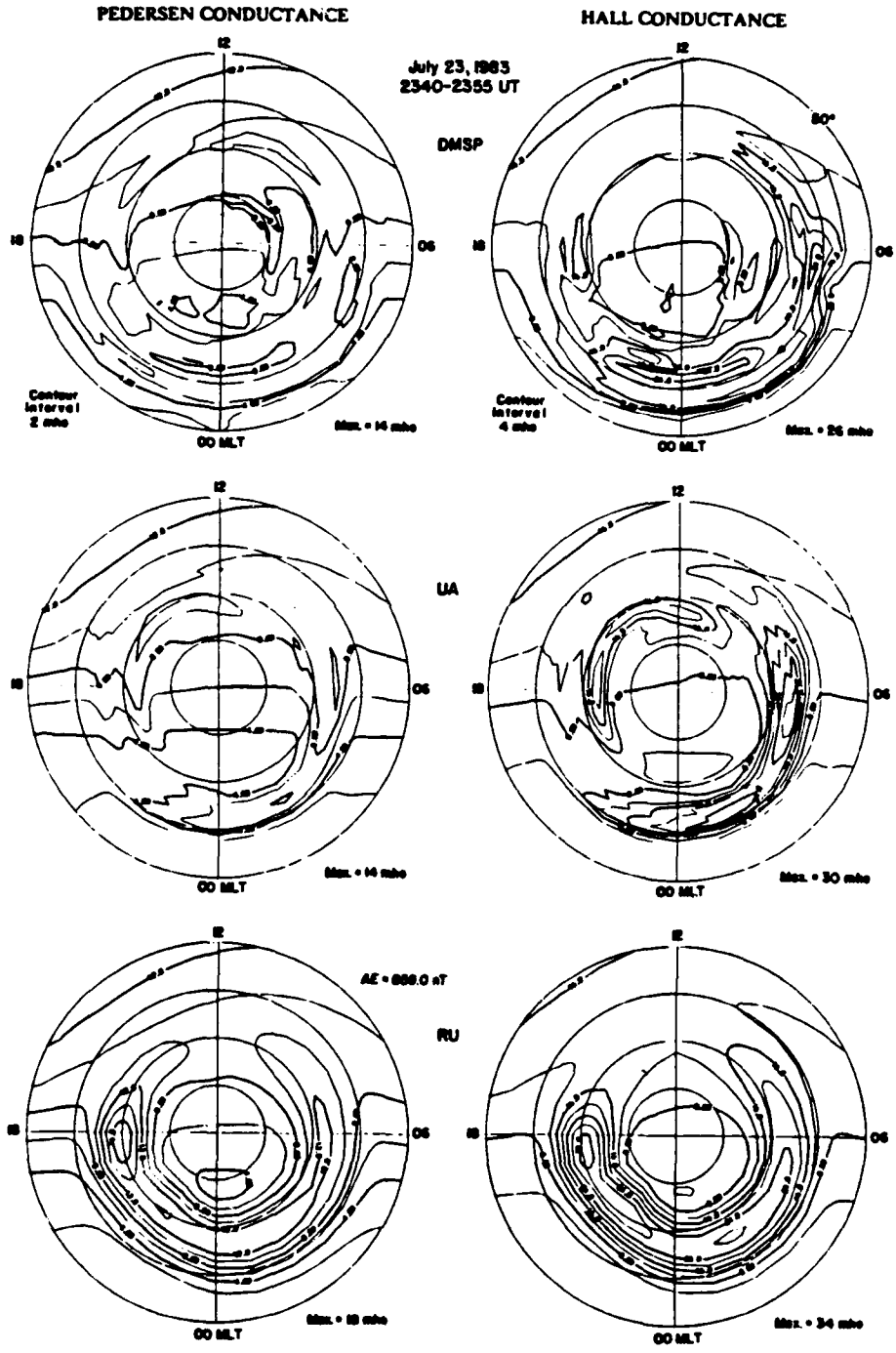

Figure 1. Isocontours of the Pedersen and Hall conductance distributions based on the DMSP data, and UA and RU conductance models at 2340-2355 UT on 23 July 1983. The contour intervals for Pedersen and Hall conductance are 2 and 4 mhos, respectively. The maximum conductance value of each distribution is shown in the bottom right corner of the corresponding panel.

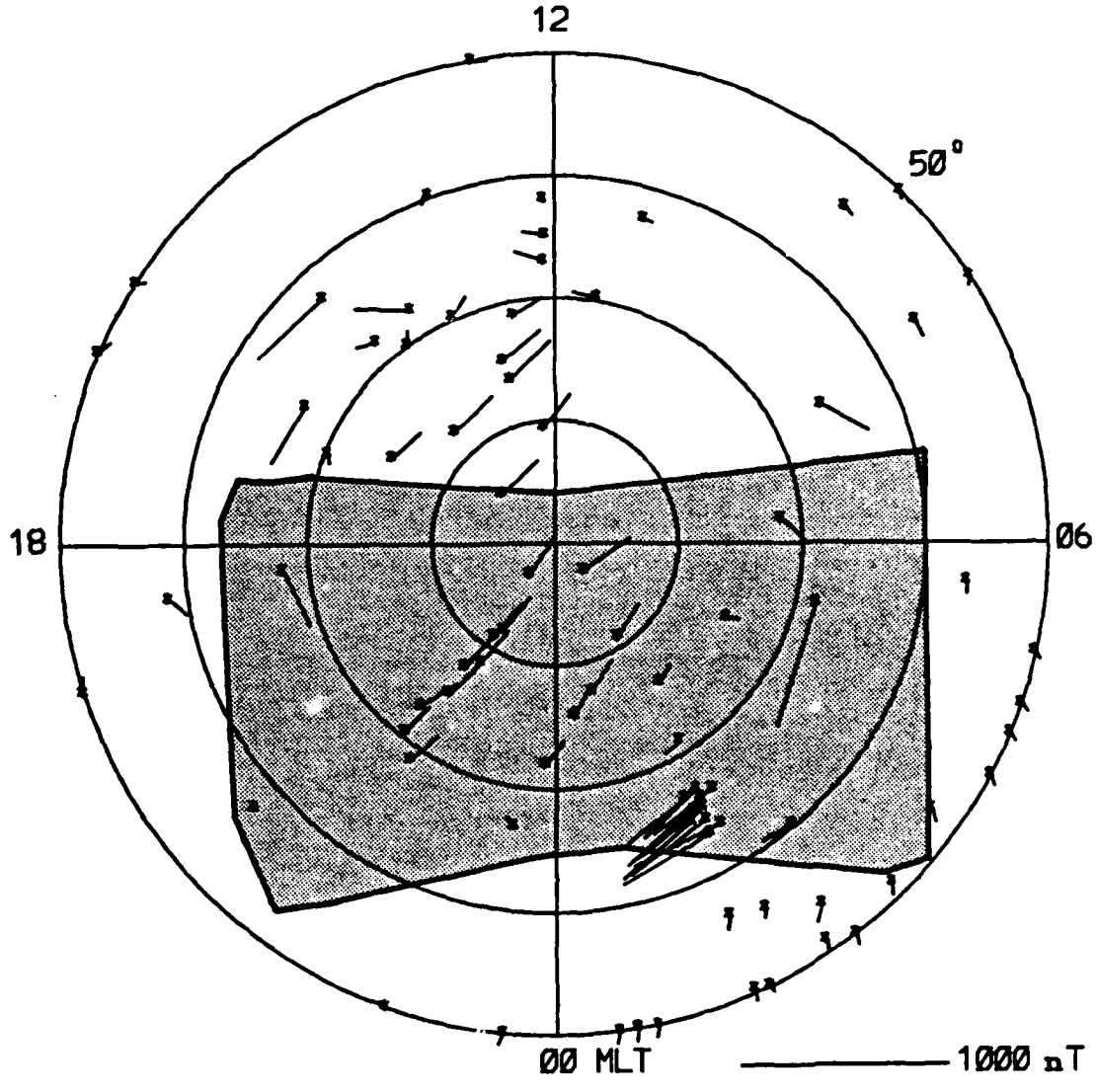

Figure 2. Magnetic perturbation vector observed from 88 stations in the northern hemisphere at 2340-2355 UT on 23 July 1983. The shaded area represents the field of che X-ray imager.

interesting differences are noticeable. In particular, the most enhanced regions of both the Hall and Pedersen conductance distributions of the DMSP-based and the UA models are located in the midnight-morning sector, but they are found in the dusk sector in the RU model. There are a number of small-scale structures in the DMSP-based and UA models which do not appear in the statistical RU model.

3. CASE STUDY

Our input for the calculation of Φ and U consists of the ground magnetic perturbation data from 88 magnetic observatories in the northern hemisphere for two consecutive days, 23-24 July 1983, and the conductance distributions. During the interval, there were a number of substorms, ranging from an isolated substorm to continuous substorm activity, and from small substorms to large ones. Thus this data set, with its wide range of magnetic activity, could serve as an ideal data base for correlating global ionospheric quantities and geomagnetic indices. An example of our ground magnetometer data is shown in Figure 2. The magnetic activity during the entire period is shown in the bottom panel of Figures 3 and 4 in terms of the AE(12) index. To match other quantities determined in this study, the AE(12) index is also averaged over the scanning period of the satellite, thus ignoring rapid variations.

The computer code employed in this study is an improved version of that developed by Kamide et al. (1981), referred to as the KRM algorithm. With the data set and the computer code, various ionospheric quantities, e.g., ionospheric currents, field-aligned currents, the electric potential, and the Joule heating rate have been obtained (Ahn et al. 1986). However, the present report considers only two scalar quantities, i.e., the electric potential and the Joule heating rate, which have been reported to be highly dependent upon the choice of ionospheric conductance distribution (Kamide and Richmond 1982).

The left side of Figure 5 shows the electric potential distributions at 2340-2355 UT on 23 July 1983, based on the three different conductance distributions: DMSP-based (top), UA model (middle), and RU model (bottom). All three patterns, basically consisting of two convection cells with a signature of the intrusion of the morning cell into the evening sector (Yasuhara et al. 1983; Kan and Kamide 1985), have similar global-scale features. There are, in fact, remarkable similarities in the sunlit hemisphere, where the conductance is dominated by the solar UV radiation, so no significant difference is expected from one conductance distribution to another. On the other hand, one can see considerable differences on the night side. Note the unusually strong potential structure in the premidnight sector below 60° latitude of the bottom

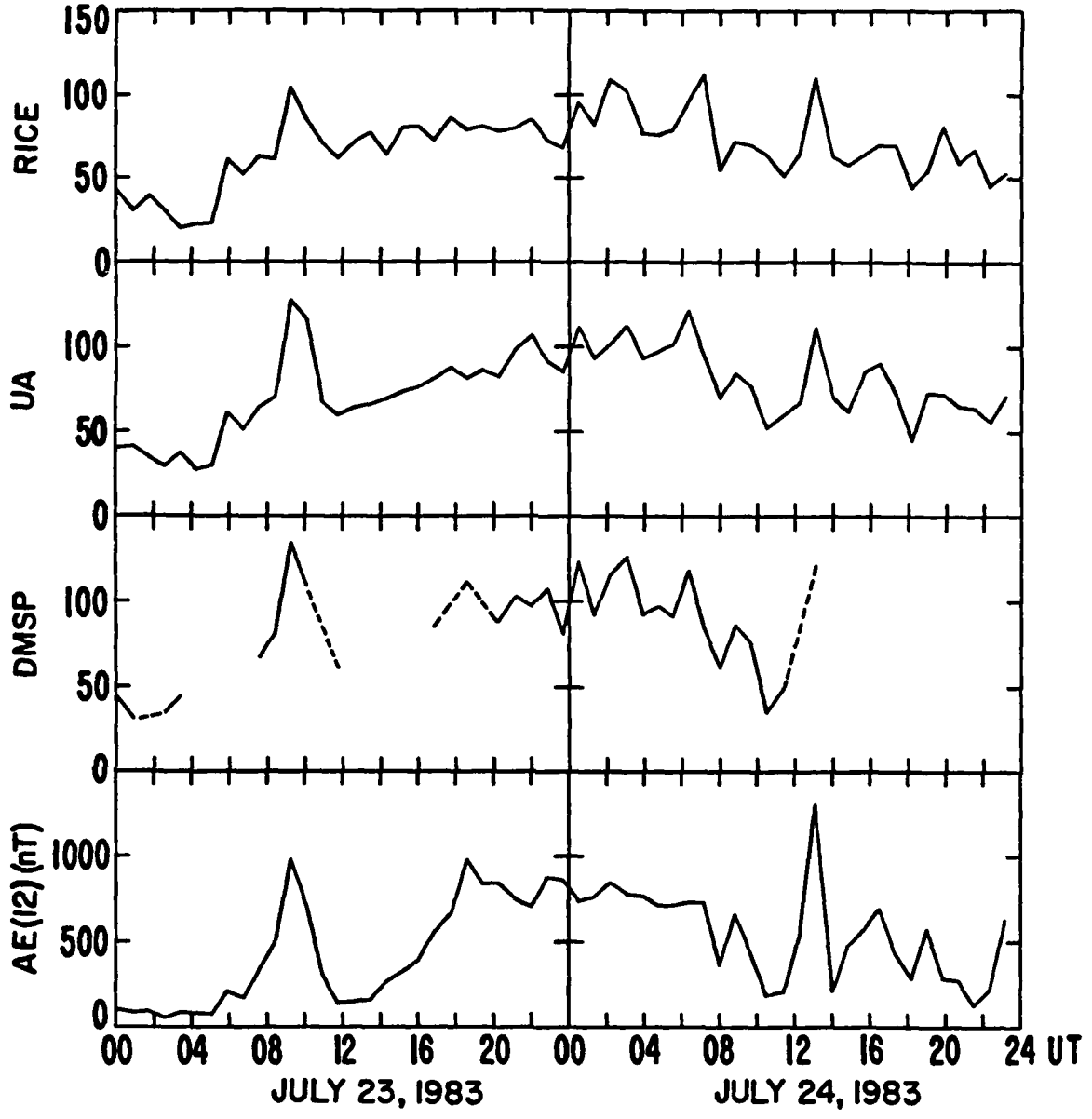

Figure 3. Comparison between the cross-polar cap potential differences based on the three conductance distributions along with the AE(12) index. The dotted lines in the third panel indicate missing data intervals of less than one hour.

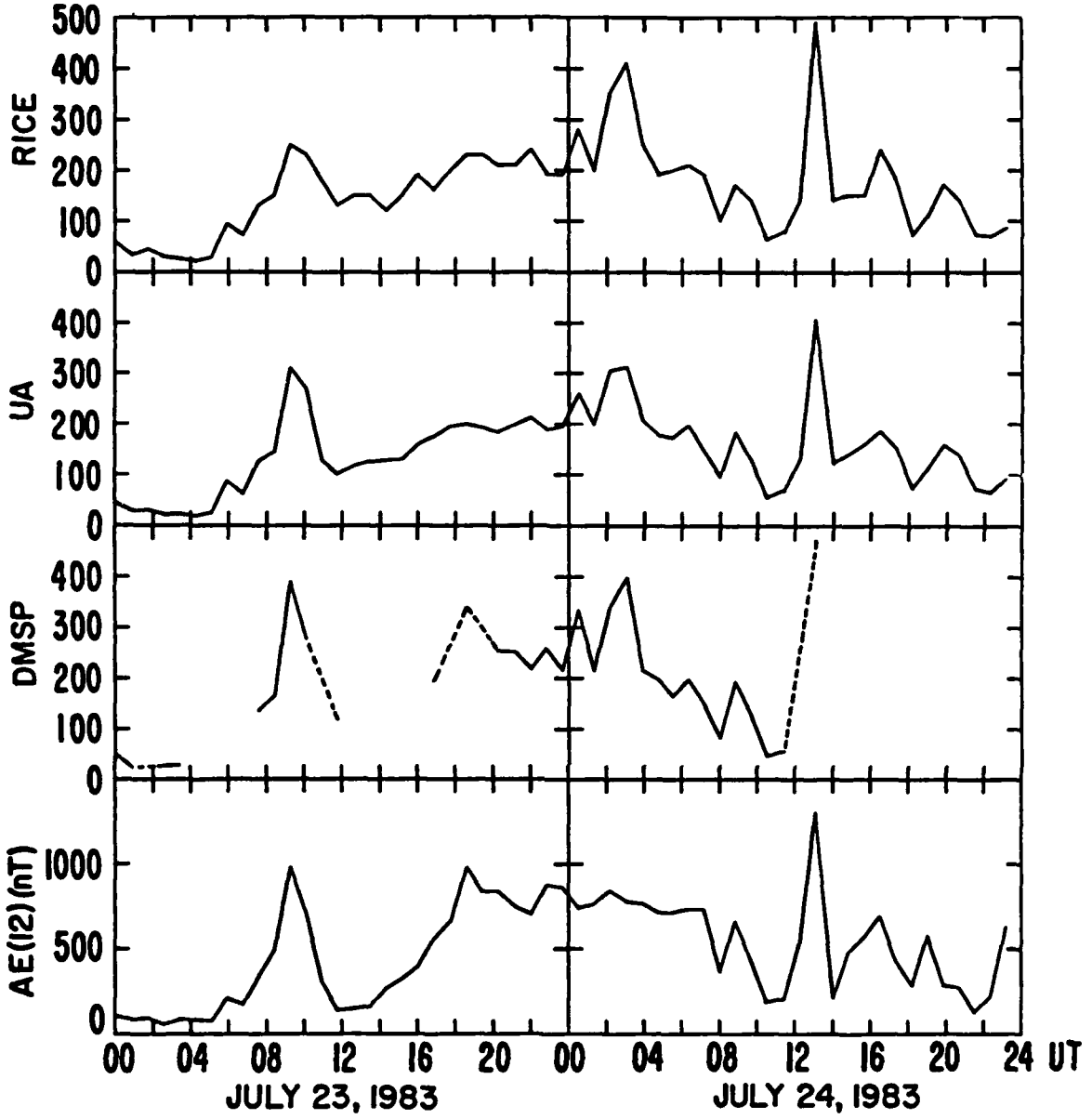

Figure 4. Same as Figure 3, but for the global Joule heating rate variations along with the AE(12) index.

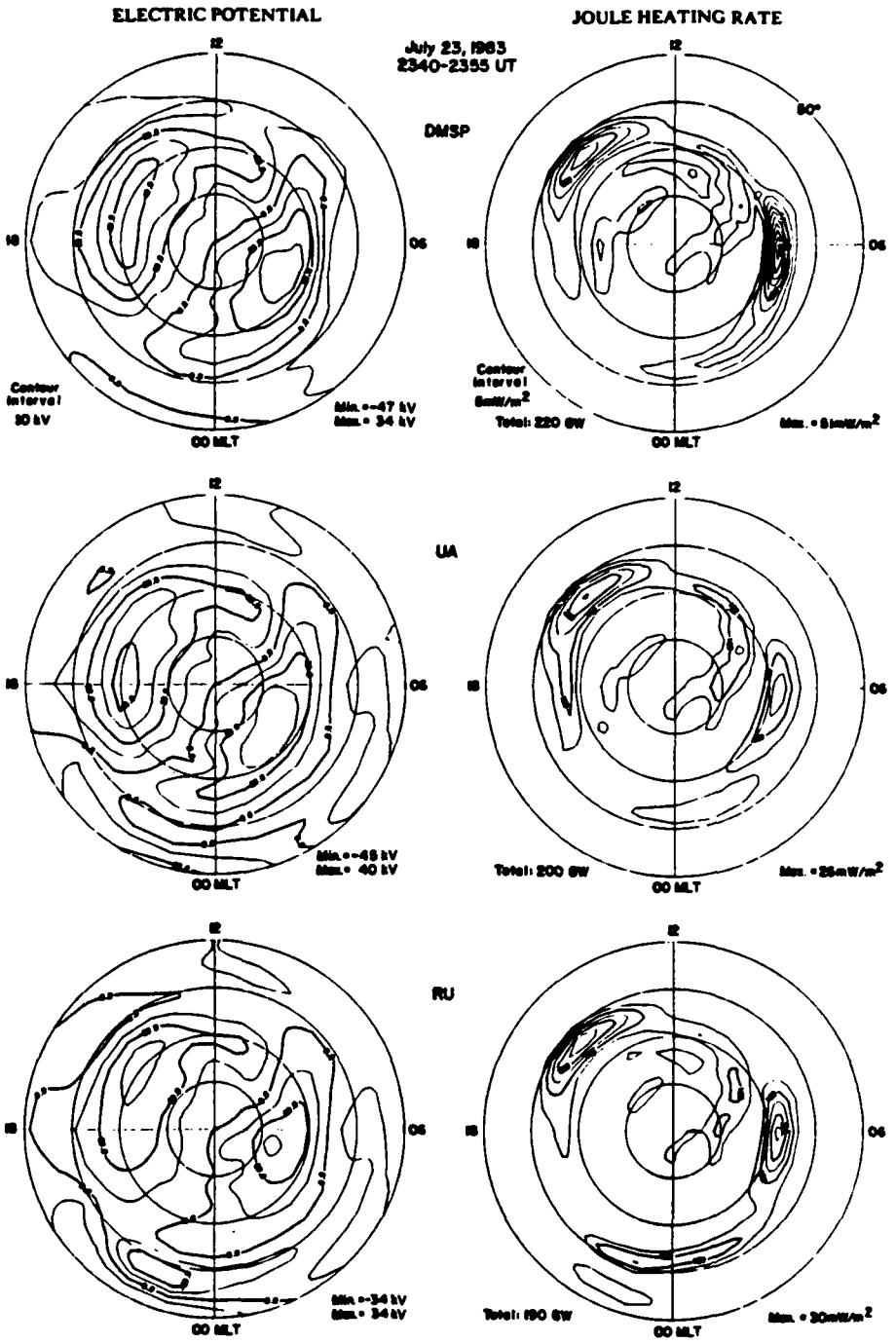

Figure 5. Electric potential distribution patterns (contour interval: 10 kV) based on the DMSP data; the UA and RU model for the same epoch with Figure 2 are shown in the left hand side. The maximum and minimum potential values are denoted in the bottom right corner of each panel. Also shown are the corresponding Joule heating rate distributions (contour interval: 5 mW/m^2). The global Joule heating rate and the maximum Joule heating rate are found in the bottom left and right corners, respectively.

panel in Figure 5, which is based on the RU model, while no such signature is found in the top panel based on the actual DMSP measurements. Kamide et al. (1982a) have pointed out that such unusual potential structures at a lower latitude are probably not real and are caused by the unrealistic assumption adopted in the KRM algorithm that the geomagnetic field lines are effectively radial. It seems quite conceivable, however, that they are associated more closely with the unrealistic conductance distribution of the region than with the assumption.

The cross-polar cap potential difference is calculated by simply taking the difference between the highest and the lowest potential values, which are generally located in the dawn and dusk sectors, respectively. These extreme values, in kilovolts are shown in the bottom right corner of each panel. In determining the extreme value of the potential distribution, however, one should be cautious, since sometimes it appears below 60° in latitude as frequently happens in our examples, particularly the one based on the RU model (Kamide et al. 1983). The cross-polar cap potential differences thus obtained, for the examples shown in Figure 5, were 81, 85, and 64 kV based on the DMSP data, and the UA and RU models, respectively. The order of magnitude of Φ estimated through magnetometer inversion method, regardless of the conductance distribution employed, is quite comparable to other estimations based on completely different principles (Reiff et al. 1981, 1985).

The right-hand side of Figure 5 shows the distributions of the Joule heating rate at 2340 to 2355 UT on 23 July 1983, based on the three conductance distributions in Figure 1. The three distribution patterns are remarkably similar as far as their global features are concerned. Although the ionospheric current distribution is not shown here, the major Joule heating regions in the dawn and dusk sector are closely associated with the auroral electrojets. However, one can notice that there are considerable differences in small-scale structures, particularly in the midnight-morning sector. Note that both of the maximum heating regions based on the statistical conductance models are located in the afternoon sector, while the one based on DMSP data is found in the morning sector. Moreover, the magnitude of the maximum heating rate of the latter, shown in the bottom right corner of each panel, is larger than those based on the statistical models;

compare the conductance distribution patterns of the region in Figure 1. Recently growing evidence indicates that the electric field enhancement is more important than the ionospheric conductance enhancement in the poleward half of the westward electrojet in the morning sector, while the opposite is true in the equatorward half of this electrojet (Senior et al. 1982; Kamide and Vickrey 1983; Foster 1987). If this is indeed the case, the underestimation of the Joule heating rate or the overestimation of the ionospheric conductance in the poleward half of the westward electrojet in the morning sector is inevitable, since the presently available conductance models are constructed to simulate the same degree of enhancement for both the poleward and equatorward halves of the electrojets with a Gaussian profile. In spite of such a discrepancy, it is still worthwhile to mention that the Joule heating rates estimated through the magnetogram-inversion method, no matter which conductance distribution is employed, are comparable in magnitude with more direct estimations, for example, by the Chatanika radar (Wickwar et al. 1975; Banks et al. 1981; Vickrey et al. 1982), and with satellite measurements (Foster et al. 1983; Rich et al. 1987). Furthermore, all three distribution patterns share the common feature that no significant Joule heating is registered in the local midnight sector, consistent with previous studies (Banks 1977, Vickrey et al. 1982; Kamide and Baumjohann 1985).

The global Joule heating rate U is obtained by integrating the Joule heating rate from 50° latitude to the pole. Note that the contribution from below 50° can be neglected (Ahn et al 1983a). For this purpose, the polar ionosphere is divided into 960 cells spaced 1° latitude and 15° in longitude from the pole to 50° latitude. The global Joule heating rates U (one hemisphere) thus obtained at 2340 to 2355 UT on 23 July 1983, based on the two conductance models, were 200 GW for the UA model and 190 GW for the RU model, while U was 220 GW for the DMSP-based conductance distribution. The comparability among the three different estimations of U clearly suggests that the global quantity is less sensitive to the choice of conductance distribution than Φ is. On the other hand, they are also quite comparable with other presently available estimations (Akasofu 1981; Banks et al. 1981; Nisbet 1982; Bleuler et al. 1982) in terms of the order of magnitude.

4. STATISTICS

A. CROSS-POLAR CAP POTENTIAL DIFFERENCE

Figure 3 shows the cross-polar cap potential difference Φ for the two-day interval based on the three different conductance distributions along with the AE(12) index. As mentioned earlier, the ground magnetometer data were averaged over the satellite scanning period of about 17 min. The AE(12) index was also processed accordingly, thus resulting in a smooth-looking trace in the bottom panel. The first and second panels show the Φ variations, based on the RU and UA conductance models, respectively. The third panel depicts the variations based on the actual satellite measurement. A total of 30 X-ray images were available during the two-day interval, including those obtained over the southern polar region based on the assumption of a marked auroral conjugacy between the northern and southern hemispheres (Akasofu 1977, and references therein; Mizera et al. 1987). The dotted traces are used wherever missing data intervals of less than one hour are encountered. In spite of the data gap in the variations from the actual measurements, one can see that the four traces are fairly well correlated with each other, regardless of the different conductance models employed. It is interesting to see that when AE activity is low, as in the 00-04 UT July 23 interval, the three conductivity models give 30 ~ 40 kV in Φ as the quiet-time potential drop from which substorm values deviate.

For a quantitative comparison between Φ's based on different conductance models, scatter diagrams for Φ(RU) - Φ(DMSP) and Φ(UA) - Φ(DMSP) are constructed and shown in the top and bottom panels of Figure 6, respectively. One can notice that there exist remarkable linearities in both cases, with correlation coefficients of 0.87 for the top and 0.94 for the bottom panels, suggesting that the two statistically determined conductance models can be used as a first approximation, as far as a global quantity Φ is concerned. On the other hand, the linear regression lines for both cases are also estimated i.e., $\Phi(RU) = 0.85 \cdot \Phi(DMSP)$ and $\Phi(UA) = 0.96 \cdot \Phi(DMSP)$. The smaller slope (0.85) of the Φ(RU) versus Φ(DMSP) relation indicates that Φ(RU) is slightly underestimated.

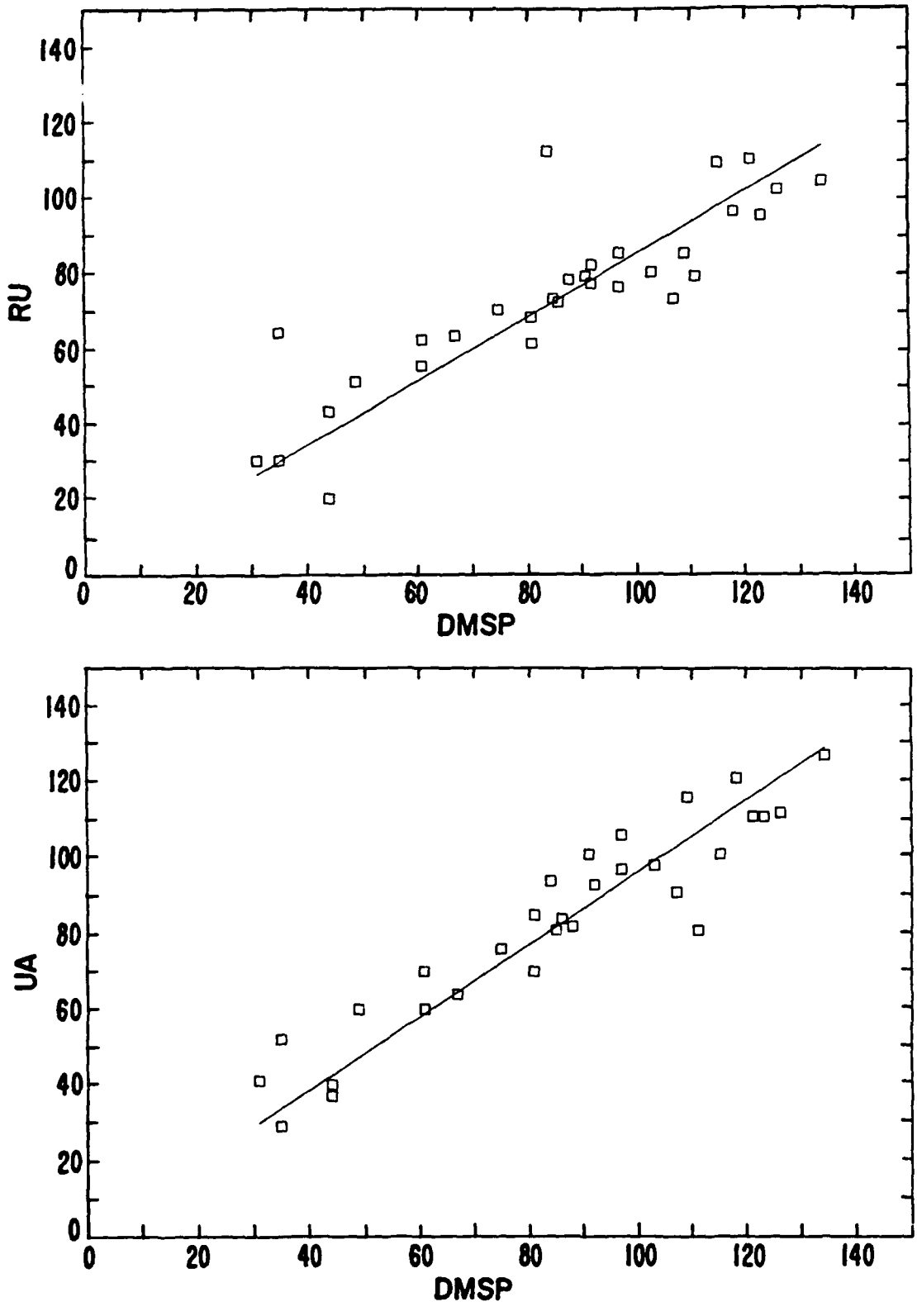

Figure 6. Scatter diagrams showing the relationship between the cross-polar cap potential differences based on the three conductance distributions. The top and bottom panels show Φ(RU) - Φ(DMSP) and Φ(UA) - Φ(DMSP) relationships, respectively.

B. GLOBAL JOULE HEATING RATE

Figure 4 shows the global Joule heating rate U based on the three conductance distribution for 23-24 July 1983, as well as the AE(12) index during the period. As in Figure 3, U(RU) and U(UA) are estimated every 50 min, corresponding to one-half of the orbital period of the satellite, while U(DMSP) was estimated during the 30 epochs when the X-ray image data were available. Here again, one can notice that all three variations are well correlated with each other. Almost every peak appearing one trace of U is associated with the corresponding enhancement of the other traces, regardless of the conductance distribution employed. Such a trend also persisted among all three traces of U and that of the AE(12) index except for the early hours of 24 July where strong enhancements of U are registered in all three traces without corresponding enhancement of the AE(12) index.

Scatter diagrams similar to Figure 6 were prepared for the comparison between the U values based on the three different conductance distributions. The top and bottom panels of Figure 7 show the relationships of U(RU) - U(DMSP) and U(UA) - U(DMSP), respectively. The linearities between them are slightly better than those shown in Figure 6 in terms of the correlation coefficient, with 0.94 for U(RU) - U(DMSP) and 0.95 for (UA) - U(DMSP), suggesting that the global Joule heating rate is less sensitive, although not remarkable, to the choice of the conductance model than that of the cross-polar cap potential difference. As can be seen from the linear regression lines, U(RU) = 0.92 • (DMSP) and U(UA) = 0.84 • U(DMSP); however, this improvement in linearity does not guarantee that the statistical conductance models are accurate enough in estimating the realistic global Joule heating rate in terms of the magnitude. Note that U(RU) and U(UA) registered about 92 and 84% of U(DMSP), respectively.

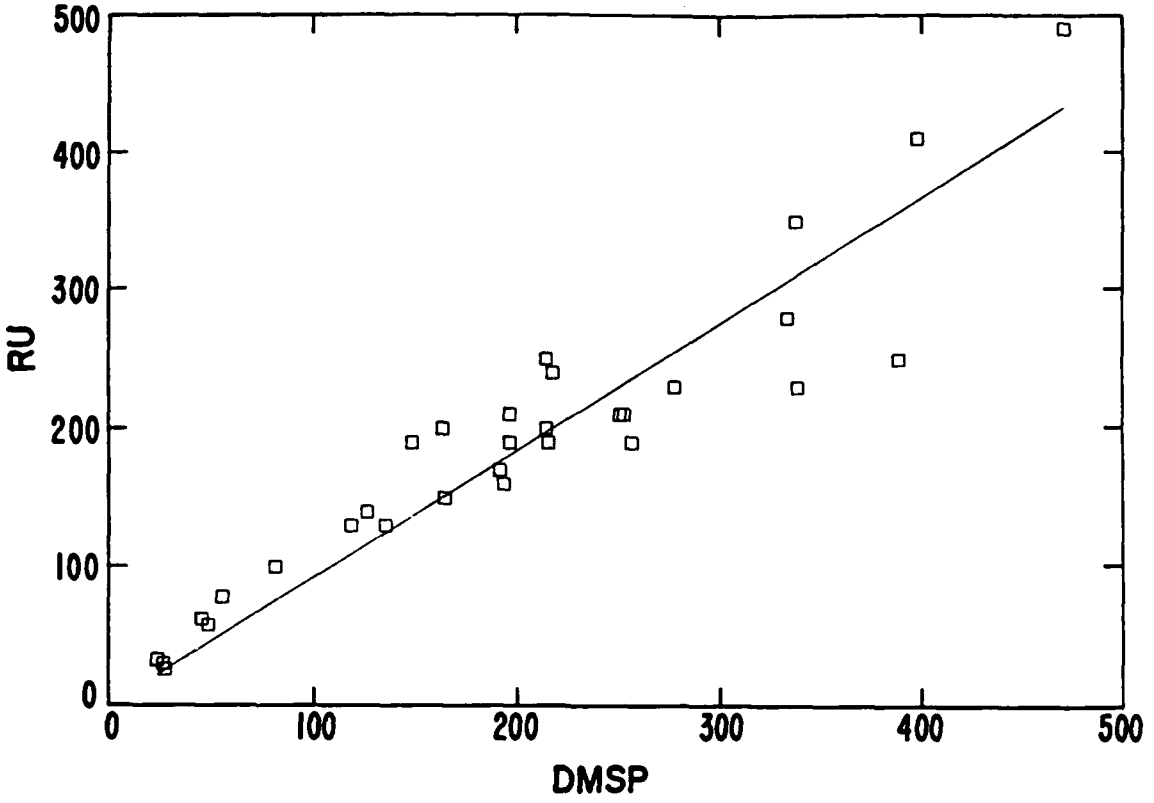

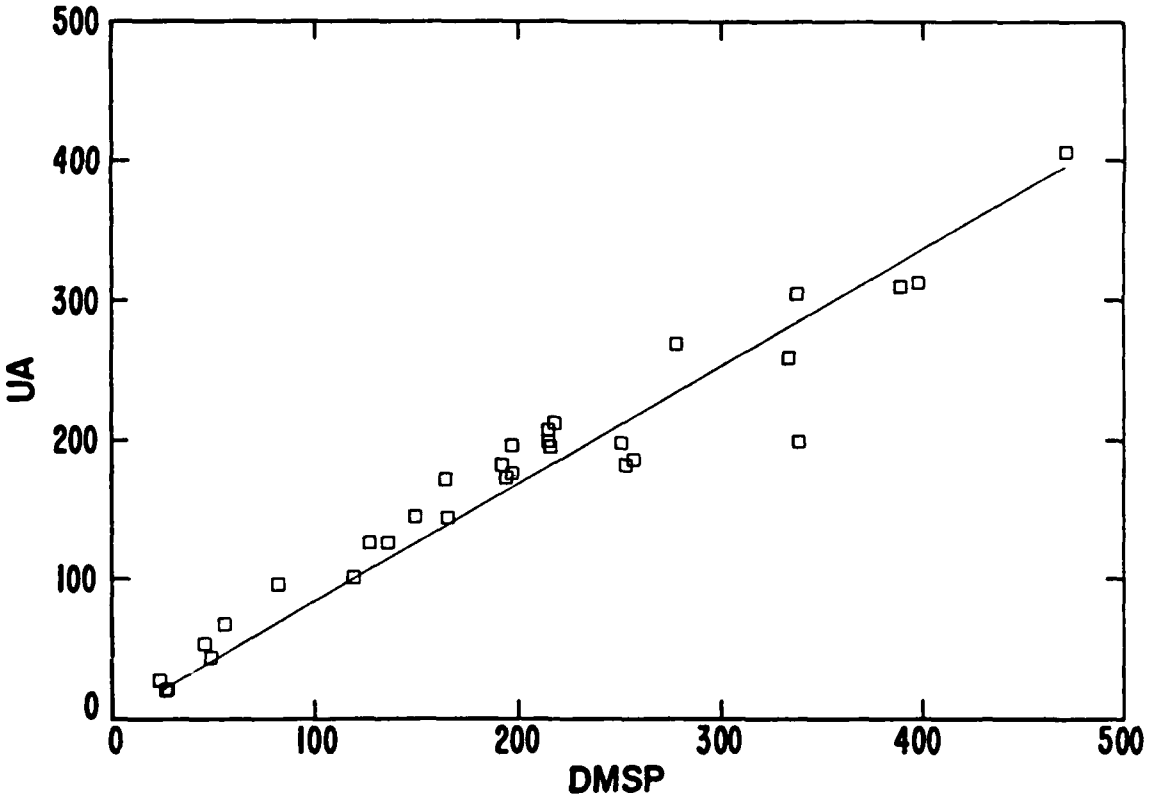

Figure 7. Same as Figure 6, but for the relationships of U(RU) - U(DMSP) and U(UA) - U(DMSP).

5. CONCLUSIONS AND DISCUSSION

The cross-polar potential difference Φ and the global Joule heating rate U are estimated from the ground magnetometer data of 23 and 24 July 1983, using two statistically determined conductance models and a realistic conductance distribution estimate from DMSP X-ray image data through the KRM method. Although we have not tested all the available conductance models, we can still draw some conclusions about the effects of the choice of conductance models on the estimations of Φ and U and the implication of correlation studies of these quantities obtained with the geomagnetic indices. The quantities Φ and U are generally enhanced, regardless of which conductance distribution is employed, as the magnetic activity increases. Recently, several studies have noted such linear relationship between Φ and the AE index (Ahn et al. 1983a; Baumjohann and Kamide 1984), using completely different data base and principles. Unfortunately, so far there has been no way to evaluate the errors involved in such studies, since the conductance models employed cannot be tested on a global scale against a realistic conductance distribution.

In spite of some shortcomings, particularly in the global coverage, which limited some of our conclusions, the conductance distribution based on the DMSP X-ray image data provides a unique opportunity for such a test. The remarkably high linearities shown in Figures 6 and 7 indicate that the two statistical models can be used as a first approximation as far as such global quantities as Φ and U are concerned and can consequently gauge the reliability of the results of the correlation studies mentioned above, which were based on one of the presently available conductance models. The conclusion is particularly important given that we have to rely on one model or another in estimating Φ and U, etc., since a realistic conductance distribution is usually not available.

On the other hand, it is appropriate to mention that there are several problems that might be taken into account in constructing a better statistical conductance model in the future. First, as can be seen from Figures 6 and 7,

there is a tendency for both Φ and U based on the statistical models to be somewhat underestimated compared to those based on the DMSP data, thus indicating that the conductance values of both models are overestimated. The possibility of overestimation has already been addressed by Vickrey et al. (1981) and Robinson et al. (1987). Second, as important as estimating ionospheric conductance value in a conductance model is finding the locations of enhanced conductance regions. In the two models employed in this study, the enhanced conductance regions with a Gaussian profile are collocated with the enhanced ionospheric current belts. The basic idea behind such positioning is that the ionospheric current enhancement is accompanied closely by the ionospheric conductance enhancement at all local times. However, recently there has been evidence that the ionospheric conductance and the electric field play different roles in the enhancement of the ionospheric current at different local time sectors (Senior et al. 1982; Kamide and Vickrey 1983; Foster 1987; Ahn et al 1988). In particular, this tendency seems to be prominent in the morning sector. Note that the enhanced Hall conductance regions in the morning sector of the two models shown in Figure 6 are located at a slightly higher latitude zone than the one in the same sector of the DMSP conductance distribution. The two aspects mentioned above can be improved by employing the revised formula for conductance estimation and taking into account the local time effect on the conductance enhancement. Third, there seems to be another aspect of the relative importance in a temporal sense: the electric field enhancement is more important than the ionospheric conductance enhancement during the early phase of a substorm, whereas the opposite trend persists during and after the maximum phase (Kamide and Baumjohann 1985; Ahn et al 1988). If this is really the case, it is not easy to improve the presently available conductance models, which use ground magnetometer data directly or indirectly in terms of geomagnetic indices, since they are a combined effect of the ionospheric conductance and electric field.

REFERENCES

Ahn B. -H., Akasofu S. -I. and Kamide Y.	1983a	J. Geophys. Res. 88, 6275.
Ahn B. -H., Akasofu S. -I., Kamide Y. and King J. H.	1984	J. Geophys. Res. 89, 11028.
Ahn B. -H., Kamide Y. and Akasofu S. -I.	1986	J. Geophys. Res. 91, 5737.
Ahn B. -H., Kroehl H. W. Kamide Y. and Gorney D. J.	1988	J. Geophys. Res. 8?, (submitted for publication)
Ahn B. -H., Robinson R. M., Kamide Y. and Akasofu S. -I.	1983b	Planet. Space Sci. 31, 641.
Akasofu S. -I.	1977	Physics of Magnetospheric Substorms, p. 81, D. Reidel, Hingham, Mass.
Akasofu S. -I.	1981	Space Sci. Rev. 28 121.
Akasofu S. -I. and Kamide Y.	1985	EOS, 66, 465.
Banks P. M.	1977	J. Atmos. Terr. Phys. 39, 179.
Banks P. M., Foster J. C. and Doupnik J. R.	1981	J. Geophys. Res. 86., 6869
Baumjohann W. and Kamide Y.	1984	J. Geophys. Res. 89, 383.
Bleuler E., Li C. H. and Nisbet J. S.	1982	J. Geophys. Res. 87, 757.
Craven J. D., Kamide Y. Frank L.A., Akasofu S.-I. and Sugiura M.	1984	Magnetospheric Currents (Potemra T. A., Ed) Vol. 28, p. 137, AGU, Washington, D. C.
Foster J.C.	1987	Geophys. Res. Lett. 14, 160.
Foster J.C., St. -Maurice J. -P and Abreu V. J.	1983	J. Geophys. Res. 88, 4885
Fuller-Rowell T. J. and Evans D. S.	1987	J. Geophys. Res. 92, 7606.
Hardy D. W., Gussenhoven M. S., Raistrick R. and McNeil W. J	1987	J. Geophys. Res. 92, 12275.
Jmhof W. L., Nakano G. H., Johnson R. G. and Reagan J. B.	1974	J. Geophys. Res. 79, 565.

Imhof W. L., Voss H. D. Datlowe D. W. and Mobilia J.	1985	J. Geophys. Res. 90, 6515.
Imhof W. L., Voss H. D. Datlowe D. W. and Mobilia J.	1988	J. Geophys. Res. 93, 2649.
Kamide Y., Ahn B. -H., Akasofu S. -I., Baumjohann W., Friis-Christensen E., Kroehl H. W., Maurer H., Richmond A. D., Rostoker G., Spiro R. W., Walter J. K. and Zaitzev A. N.	1982a	J. Geophys. Res. 87, 8228.
Kamide Y., and Baumjohann W.	1985	J. Geophys. Res. 90, 1305.
Kamide Y., Craven J. D., Frank L. A., Ahn B. -H. and Akasofu S. -I.	1986	J. Geophys. Res. 91, 1235.
Kamide Y., Kroehl H. W., Hausman B. A., McPherron R. L., Akasofu S. -I., Richmond A. D., Reiff P. H. and Matsushita S.	1983	WDC-A Report UAG-88, Boulder, Colorado.
Kamide Y., Kroehl H. W., Richmond A. D., Ahn B. -H. Akasofu S. -I., Baumjohann W., Friis-Christensen E., Matsushita S., Maurer H., Rostoker G., Spiro R. W., Walker J. K. and Zaitzev A. N.	1982b	WDC-A Report UAG-87, Boulder, Colorado.
Kamide Y., and Matsushita S.	1979	J. Geophys. Res. 84, 4083.
Kamide Y., and Richmond A. D.	1982	J. Geophys. Res. 87, 8331.
Kamide Y., Richmond A. D., and Matsushita S.	1981	J. Geophys. Res. 86, 801.
Kamide Y., Robinson R. M. Akasofu S.-I and Potemra T. A.	1984	J. Geophys. Res. 89, 389.
Kamide Y., and Vickrey J. F.	1983	J. Geophys. Res. 88, 7989.
Kan J. R. and Kamide Y.	1985	J. Geophys. Res. 90, 7615.
Mishin V. M., Lunyushkin S. B. Shirapov D. S. and Baumjohann W.	1986	Planet Space Sci. 34, 713.
Mizera P. F., Gorney D. J. and Evans D. S.	1987	Geophys. Res. Lett. 4, 190.

Mizera P. F., Gorney D. J. and Roeder J. L.	1984	Geophys. Res. Lett. 11, 255.
Mizera P. F., Kolasinski W. A., Gorney D. J. and Roeder J. L.	1985	J. Spacecraft and Rockets 22, 514.
Mizera P. F., Luhmann J. G. Kolasinski W. A., and Blake J.B.	1978	J. Geophys Res. 83, 5573.
Nisbet J. W.	1982	J. Atmos. Terr. Phys. 44, 797.
Rich F. J., Gussenhoven M. S. and Greenspan M. E.	1987	Ann. Geophysicae 5A, 527.
Reiff P. H., Spiro R. W. and Hill T. W.	1981	J. Geophys. Res. 86, 7639.
Reiff P. H., Spiro R. W., Wolf R.A., Kamide Y. and King J. H.	1985	J. Geophys. Res. 90, 1318.
Robinson R. M., Vondrak R. R. Miller K., Dabbs T. and Hardy D.	1987	J. Geophys. Res. 92, 2565.
Rosenberg T. J., Detrick D. L., Mizera P. F., Gorney D. J., Berkey F. T., Eather R. H. and Lanzerotti L. J.	1987	J. Geophys. Res. 92, 11123.
Senior C., Robinson R. M. and Potemra T. A.	1982	J. Geophys. Res. 87, 10469.
Spiro R. W., Reiff P.H. and Maher L. J. Jr.	1982	J. Geophys. Res. 87, 8215.
Vickrey J. F., Vondrak R. R. and Matthews S. J.	1981	J. Geophys. Res. 86, 65.
Vickrey J. F., Vondrak R. R. and Matthews S. J.	1982	J. Geophys. Res. 87, 5184.
Wallis D. D. and Budzinski E. E.	1981	J. Geophys. Res. 86, 125.
Wickwar V. B., Baron M. J. and Sear R. D.	1975	J. Geophys. Res. 80, 4364.
Yasuhara F., Greenwald R. and Akasofu S. -I.	1983	J. Geophys. Res. 88, 5573.